Terahertz and Optical Spectroscopy of Rare Earth-Doped Materials

A Major Qualifying Project

Submitted to the Faculty of

Worcester Polytechnic Institute

In partial fulfillment of the requirements for the

Degree in Bachelor of Science

in

Physics

By:

_____

Benjamin J. Dringoli

Date: 4/27/17

Project Advisors:

_____

Professor Richard Quimby, Co-Advisor

_____

Professor Lyubov Titova, Co-Advisor

Abstract

While rare earth-doped glasses and crystals have been studied previously, the low-energy transition dynamics of rare earth Stark levels caused by the presence of a crystal field have not. THz spectroscopy techniques present a useful tool for identifying and characterizing the low-energy intramultiplet transitions of these rare earth ions. This project acts as a road map for THz spectroscopy of this class of materials, providing background on the physics of these systems as well as introduction to the spectroscopy techniques and why they are well suited for this application. Simulations and preliminary calculations showing predicted absorption spectra were done and preliminary spectroscopic data showing the potential application of these techniques on available samples is reported. Possibilities for optimal ion-host combinations are given and absorption dynamics are simulated such that future experiments can be compared to these expected results. It is found that THz spectroscopy is a promising technique for studying these systems, and guidelines for selecting the ion, host, and excitation energy for future work are given.

Table of Contents

Introduction

Rare earth-doped crystals are materials consisting of an ion doped into a surrounding host material characterized by sharp absorption and emission lines, and have received a lot of attention due to their applications in solid state lasers as well as other devices. Furthermore, rare earth ions in crystal hosts exhibit another interesting effect caused by their two-part nature: the very fine splitting of degenerate energy states, known as the Stark effect. This arises because well shielded electrons in the ion's 4f shell are slightly perturbed by the electric field from the surrounding crystal; the slight differences in the electron properties causes the normally degenerate energy states to separate. This collection of states is called a Stark manifold, and while it creates some very interesting properties due to the small energy differences between the states within, there is still little information about the dynamics surrounding these states. The positions and transition dynamics of these energy states are determined by the properties of both the ion and the host, and therefore choosing the right ion-host combination and modeling the effects of this choice are important. Thus this project focuses on the choice of material, modeling of absorption dynamics and material properties, and preliminary experimental testing.

Identifying these transitions could be a gateway to many new applications of these materials; probing the effects of different ion-host combinations may allow for more specialized materials can be constructed. Also, characterizing dynamics of intramultiplet transitions is important for assessing applicability of rare earth doped crystals and glasses in high speed applications in the far-IR.

Up until recently, there have been very few reliable methods to probing the interactions and dynamics involving these low energy transitions. Optical techniques had not advanced far

enough into the far-IR frequency range when these materials were heavily studied and electronics have just been able to surpass GHz frequencies. This left a void in the available frequencies for spectroscopic and electronic measurements known as the "Terahertz (THz) Gap". With the refinement of nonlinear optical techniques and with high power femtosecond lasers becoming more and more widespread, a new realm of spectroscopy has opened up in the THz region. The techniques used to accomplish this fall under the broad umbrella of Terahertz Spectroscopy, but this project will focus on using two specific procedures: THz Time-Domain Spectroscopy (THz-TDS) and Time-Resolved THz spectroscopy (TRTS). These allow for the characterization of the THz properties of the unexcited material as well as the excited state dynamics of the material. Exploiting short (<ps) duration THz pulses also allows us to study excited state dynamics by varying the delay between the optical excitation and the THz probe pulse.

While a few studies of THz absorption in rare earth systems using traditional far-IR methods have been reported ([1] [2] [3]), systematic study of intramultiplet transitions in the THz range is still lacking. The goal of this project is to identify the most promising ion-host combination for both TDS and TRTS tests of multiplet dynamics and produce preliminary expected as well as experimental results. We accomplish this goal by combining numerical simulations of the processes involved as well as characterization of optical and THz absorption for several rare earth doped glasses using optical and THz spectroscopy.
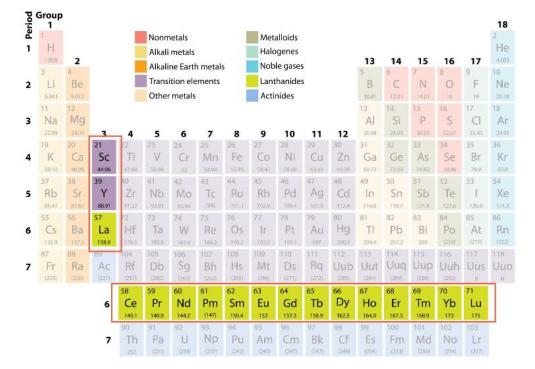
Background

Materials

Ion

Figure 1: The periodic table with the Rare-Earth/Lanthanide group highlighted (1).

Rare-earth doped crystals and glasses have been of interest in the optics community for some time due to their practical uses, particularly in lasers and photonics. The ions themselves, which could come from the lanthanide family (Z = 58-71) or the actinide family (Z = 90-103), are the most important component, as many of the material's properties will stem from the choice of dopant. This group of elements is shown in Figure 1. Rare-earth ions have many traits that distinguish them from other classes of materials: narrow absorption/emission features,

transition energies that are relatively independent of host choice, long metastable state lifetimes, and high quantum efficiencies [4]. For most optical uses, lanthanides are more widely studied and implemented, so they will be the focus for the rest of this discussion.

The lanthanides are characterized by the filling of the 4f electron shell [4]. This is important for a number of reasons; first, the 4f states are commonly shielded by the larger 5s and 5p states [5], which leads to predictable and well-resolved energy structures that are not very dependent on the host medium. Because this 4f shell is the most useful for applications and has been the most studied, many systems use trivalent ($^{3+}$) lanthanides in which the outer 6s and 5d electrons have been removed [4], which are highly stable in an insulating host. Thus the transitions of interest can either be between 4f states or possibly between 4f and 5d states depending on how the surrounding environment mixes these orbitals [5]. Transitions between 4f states are of the same parity and therefore are only dipole allowed for relatively weaker magnetic-dipole transitions, while electric-dipole transitions are allowed to the higher 5d states. Weaker electric-dipole transitions become allowed for the 4f transitions only by the small admixing of higher 5d states into the 4f states due to the local electric field. The 4f transitions are generally in the visible/infrared range, so these have been the most studied by laser physicists originally investigating these materials. This abundance of previous work makes these states the most pertinent for the goals of this project.

In the simplest view, these ion energy states would be determined by the single-electron picture in which each electron acts independently with a nucleus of effective charge Z_{eff}. However, there are a few effects that can perturb the location of atomic energy levels. We start by discussing the ones that take place within the ion: the electrostatic interaction and spin-orbit coupling.

The electrostatic interaction comes from the non-negligible interference between electrons within the same atom. Electrons will repel and exert torques on each other depending on their position and energy state, which will shift the energy levels of the atom compared to an analysis that only takes into account the electron's interaction with the positively charged nucleus. Spin-orbit coupling arises from the interaction between the electrons' orbital angular momentum and spin angular momentum. The total orbital angular momentum vector is represented by L, and it denotes the possible vector combinations of all the valence electron angular momenta l. These take the values 0, 1, 2, 3, ... which represent the type of orbit: $l = 0$ corresponds to s orbitals, $l = 1$ corresponds to p, etc. The total spin angular momentum is represented by S, and it denotes the possible vector combinations of the individual electron spins s. It takes on values in multiples of ½. The vector combination of these L and S vectors produces the total angular momentum J, and these J values label the multiplet levels produced by spin-orbit coupling [6]. While L and S are not guaranteed to be 'good' quantum numbers (i.e. are not true eigenvalues of the system), J is always a good quantum number, as would be expected for a system with spherical symmetry. Thus the original degeneracy caused by the large 1/r central potential has been split by both the electrostatic interaction between electrons (LS coupling) and a further splitting due to spin-orbit coupling. The final perturbation, called the Stark effect, splits the energy of each J level into fine multiplets. This splitting scheme is shown in Figure 2; the final splitting of the energies into Stark multiplet levels are the levels that will be studied in this project. As this effect is caused by the surrounding host field, they will be discussed in further detail in the following section.
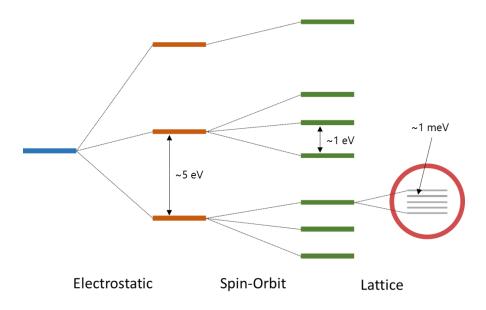
Figure 2: Energy level diagram showing the progressive splitting due to various perturbations of the ion atom and characteristic energies between split levels.

Host

As stated before, the shielding in lanthanides restricts the host properties from largely affecting many of the atomic transition properties, but there are a few important qualities of the host that must be taken into consideration to understand the choice of goals and methodology for this project.

The first important host property is its optical density in the THz region. In order to see the effect of any absorption within the rare-earth dopants, a relatively strong THz signal must be able to make its way out of the sample so it can be detected. If the sample has electronic transitions or phonon (lattice vibration) modes that occur within the bandwidth of the THz pulse, it will strongly attenuate the signal. This would lead to either no signal transmission or a very low signal-to-noise ratio, both of which will overshadow the small shifts in intensity we are looking to see as signatures of absorption from the dopant ions.

Another host property that needs to be considered is the phase or morphology. Previous optical studies of rare-earth doped materials usually focus on two classes of host materials: glasses and crystals. The main difference between these two phases is how they are structured directly around the dopant atom. Glasses are an amorphous solid with little long-range order or symmetry, which leads to each doped ion being exposed to a slightly different local environment. Even though the energy levels of the ions are well-shielded from their environment as explained above, this does not prevent the fine structure from being slightly perturbed. When this effect is averaged over a large volume and therefore a large number of individual ions, the differences in these shifts leads to a broadening of the absorption/emission features [7]. This effect, known as inhomogeneous broadening, is not present in crystalline hosts because the highly ordered crystal structure allows for each ion site to be mostly identical (barring impurities and defects). This leads to very little variation in the environment and therefore very little variation in the relative positions of energy levels between the ions. Thus, the absorption spectrum in a crystal exhibits a number of very sharp, defined peaks in the absorption/emission spectrum [8]. Since this project aims to show absorption between very finely spaced energy levels, a crystal host would be ideal. A glassy host, on the other hand, would exhibit widespread broadening of the levels which might significantly wash out any small absorption characteristics from the dopant ions.

When an ion is doped into a crystalline host, there is an extra interaction on top of the electrostatic interaction and spin-orbit coupling that can affect the positions of the ions energy levels. This is usually referred to as the crystal field, or Stark, effect [9]. It arises from the non-zero electric field around the ion originating from the host atoms surrounding it. This field affects the outer electrons of the ion by splitting the energetically degenerate J states produced by spin-orbit coupling. Because the 4f rare-earth levels are mostly shielded by the 5s and 5p states

which have higher orbital radii, the effect of the crystal field on the 4f states is small in relation to the previous splittings. Generally the crystal field term is thought of as a static perturbation that separates the levels by 10-100 cm^{-1} [4]. These small splitting are the ones to be investigated in this project, and their small size is why THz spectroscopy, which utilizes low energy photons of about 7 - 67 cm^{-1}, is being explored as the main tool for probing the dynamics within.

Another parameter that could affect the influence of the crystal field, and thus the fine splitting of the energy levels, is the temperature of the sample. In addition to introducing phonons into the system and causing homogeneous broadening, thermal expansion will enlarge the crystal lattice, weakening its effect on the ion as the average distance from the host atoms increases. Since most reported data for energy levels in rare-earth doped crystals is at low temperatures to increase accuracy, it will be interesting to see how much this project's room-temperature experiments differ.

Technique

Terahertz Radiation and Spectroscopy

The Terahertz region is generally defined as being between 300 GHz and 10 THz [10], which is roughly between the microwave and mid-IR regions. Its relation to the rest of the electromagnetic spectrum is shown in Figure 3. Until two decades ago, this region was relatively unexplored due to it being too high frequency for electronics but too low frequency for the optical techniques of the time. This lead to it being known as the 'Terahertz gap'. But thanks to new technologies and techniques it has become an important regime for many practical and scientific applications. Many large-molecule vibrational modes and low energy transitions occur in the THz range, and THz methods have been used to explore and explain the origin of these resonances [11]. The details of the most general THz spectroscopy methods and how they will apply to this project are explained in brief below.
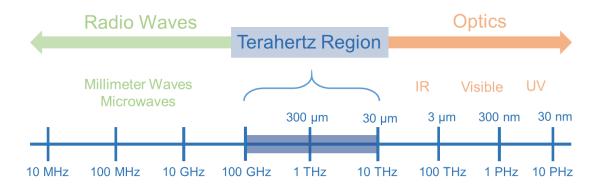
Figure 3: Electromagnetic spectrum with Terahertz gap highlighted   .

In THz spectroscopy, THz pulses generated from ultrafast laser pulses are used to study material properties. A THz pulse is a free-space propagating, approximately single-cycle electromagnetic transient with a duration of ~1 ps [11]. Because of its short duration, the pulse

has a wide bandwidth that typically extends from 0.2 to 2 THz depending on the environment, optics involved, and generation method. A typical pulse and its frequency spectrum is shown in Figure 4. This short duration and wide frequency range make THz pulses ideal for time-resolved spectroscopy measurements when there is interest in the response of a material to far-IR frequencies. Some examples of processes in the THz range are vibrational modes of large organic molecules, phonon modes in photonic crystals, free carrier absorption, as well as many others.
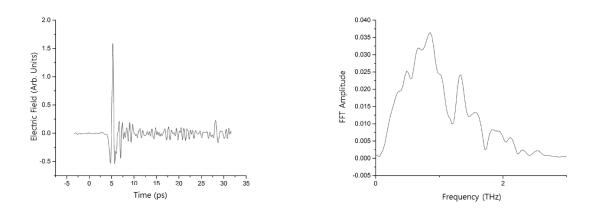

Figure 4: Time (left) and frequency (right) domain plots of a THz pulse. The dips in FFT amplitude are caused by water absorption as these measurements are done in air.

One of the most widely used techniques for generating THz pulses is the optical rectification of ultrafast optical pulses in nonlinear crystals [11]. A femtosecond laser pulse, usually in the optical frequency range, produces a polarization transient in these specialty crystals. This polarization transient then generates a THz pulse which travels out of the crystal; the electric field of this created THz pulse is proportional to the second derivative in time of the polarization transient. The material parameter that governs this effect is the second order susceptibility (χ_2), which is nonzero for materials that lack inversion symmetry. Another way of understanding this effect is to consider the frequency mixing of the incoming pulse. Ultrashort

13

(<100 fs in duration) 800 nm pulses have a bandwidth of about 15nm, and difference frequency generation between different spectral components of this pulse yield a pulse with energy in the THz range [11]. The efficiency and profile of the emitted THz pulse can be affected by a number of interactions, including phase matching conditions, interaction length, and crystal resonances. A number of crystal materials have been found that exhibit the correct traits for optical rectification such as ZnTe, LiNbO$_3$, and GaP, but ZnTe is used for the setup in this project.

Time-Domain Spectroscopy

The basis for all THz measurements is the ability to probe the sample with the THz beam and then glean material properties/responses from the transmitted radiation. The simplest application of this technique is called Time-Domain Spectroscopy (TDS) [11].
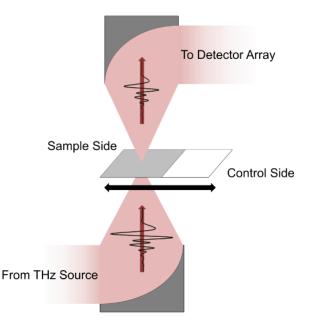

Figure 5: Diagram of the basic principle of THz-TDS showing pulse attenuation that can processed into absorption information.

The THz-TDS setup makes use of one femtosecond laser, the output of which is split into two beams. One beam is used to generate a THz pulse through optical rectification in ZnTe and

the other is sent to a delay stage to act as the sampling or gate pulse. Once the THz pulse is generated it is collimated and refocused using parabolic mirrors. Since the average frequency in the pulse is ~1 THz, which corresponds to 300 μm, the minimum spot size possible will be about 1 mm^2, although the low frequency components may take up to 2 mm^2 [11]. This focus is where the sample is placed, and after going through the sample the beam is recollimated and sent to the detection crystal. This part of the system, and how the pulse is affected, is shown in Figure 5. Here the gate pulse is used to sample the electric field of the transmitted beam through the electro-optic effect; a delay stage is used to change the time between the THz and gate pulse so the entire THz pulse (which now may be delayed/elongated) can be sampled. Optical chopping is usually used in conjunction with lock-in amplification to remove noise from the THz beam measurements [11].

To gain useful information from THz-TDS measurements, a number of trials must be done in order to compare them. Ideally, one would first compare the transmitted THz pulse through just the host material to one through air to see the effect of the pure host material. Then one would compare the pulses transmitted through both the pure and doped hosts, which provides information about the contributions of the ions. Doing these tests will allow us to ascribe various spectral features to the interaction of the THz probe pulse with the host lattice, the rare earth ions, as well as those caused by the ion-host interactions.

Time-Resolved Terahertz Spectroscopy

To observe absorption from the excited ionic states in the crystal, a slightly more advanced technique can be used that allows for the pre-excitation of the sample. This is achievable through Time-Resolved THz Spectroscopy (TRTS). Again we follow Hegmann et al.'s method and setup.

TRTS shares many traits with THz-TDS, except for the addition of a third beam that acts as an optical excitation pulse as well as another delay stage that permits delaying both THz generation and sampling beams with respect to the optical excitation [11]. Another difference between the two experimental setups is the addition of another optical chopper, this time in the optical excitation beam line. This chopper is set to double the frequency of the previous one, and allows for pump-on and pump-off measurements to be done very close to one another, minimizing any possible long-timescale changes in the material that could skew results. The results of the choppers and how they correspond to different measurement types are shown in Figure 6.
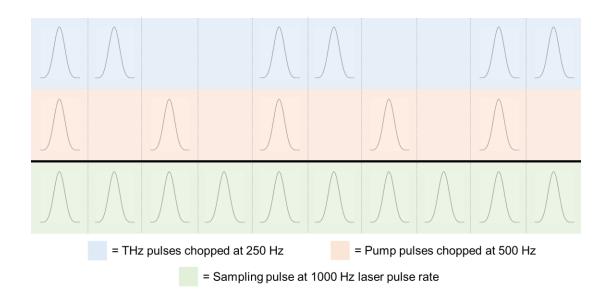

Figure 6: Pulse timing showing the ability of pump-on and pump-off measurements. Pump-on is when all three beams are allowed through, pump off is when just the THz and sampling beams are allowed. These two cases can be seen in the first two columns of the diagram.

The ability to delay the THz pulse with respect to the excitation pulse is what allows for such accurate measurements of the dynamics just after excitation. The optical pump pulse will excite ions into an upper ion manifold, then the low energy THz pulse will be absorbed if the energy difference within the now-populated Stark multiplets is within its bandwidth. Looking at

the change in transmission between pump-on and pump-off cycles will show these effects. TRTS allows one to see not only the energies in the THz regime that are absorbed, but also how they change in time, giving a complete picture of the excited state dynamics of the system.

Methodology

Spectroscopy Experiments

TDS

First, a measurement through air, with no sample on the sample stage, must be done to

determine the frequency spectra of the THz probe pulse generated in ZnTe. An example of this

pulse is shown in Figure 7. This measurement is important for finding changes between the

sample measurements as well as quantifying small changes between environmental conditions in

the lab such as temperature and humidity, which could slightly affect the nature of the laser

pulses. These measurements should start a few mm before the beginning of the pulse and extend

far enough to sample the perturbations of the pulse's tail so that all the absorption features due to

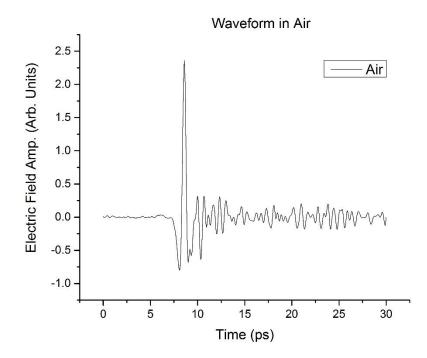the static environment can be catalogued.

Figure 7: THz pulse generated in ZnTe passing only through air.

Next, a host material without any rare-earth dopant should be placed on the sample stage and tested to show absorption information for just the host without any contributions from the rare-earth ion. These should be taken similarly to the air measurement to assure all appropriate frequency components are captured.

Finally, the rare-earth doped sample should be placed on the sample stage and tested to show the absorption of the full ion-host complex. This test is done the same as the previous two and shows the absorption of the ground state Stark multiplet, as none of the ions in the rare-earth ion have been excited. The results of this test can be compared to the host-only measurements to see if any frequency components have changed, indicating an absorption only due to the rare-earth ion concentration.

TRTS

After studying the THz absorption by the ground state multiplet of the rare-earth ion, TRTS will be used to probe absorption from the excited multiplet of the ion. Just as with the TDS measurements, transient excitation-induced changes in the THz absorption of the pure host sample will be tested first. As described above, these measurements are carried out by delaying the THz probe pulse relative to a 800 nm pump beam. Due to the low frequency chopper in the pump beam line, the data will contain both pump-on and pump-off measurements, and will allow for comparison between them, showing any changes that would result from excited state Stark transitions.

Interpreting Data

The signal from the balanced detectors is sent through lock-in detectors set to the frequencies of the beam-line choppers. This data is then sent to the computer where Labview is used to control the stages as well as collect the data. Electro-optic sampling allows us to detect an electric field vs. time profile of the THz pulse. Electric field waveforms are then transferred to the frequency domain by performing a Fourier transform, yielding amplitude and phase information. Comparing the amplitude and phase of both reference and sample pulses, we can calculate both refractive index and absorption coefficient of the studied material in the THz range. Here we will focus on the THz absorption. In the case of TRTS, we can directly obtain small excitation-induced changes to the absorption and follow these changes over picosecond timescales.

Results

Anticipated

Material Property Calculations

While preliminary spectroscopy experiments are well-suited for proof of concept tests and refining measurement techniques, an optimized doped crystal would be ideal for future tests which could show the applicability of ultrafast THz spectroscopy to probing intramultiplet absorption in rare earth ions. In order to find the material best suited for this test given the testing facilities and questions we want to answer, a literature search was done in order to find the ion-host combination that theoretically maximizes the detectable response and thus gives the best chance of successful Stark multiplet transition detection.

Of the many ions in the lanthanide family, only some would be suitable for this project. An ion with correct intermultiplet as well as intramultiplet spacing must be used in order for transition experiments to garner any meaningful results for the WPI Terahertz lab setup. To find ions that fit this criteria, the handbook Laser Crystals by Alexander Kaminskii [9] was used as a preliminary resource since it has a large list of previously studied ion-host systems and listed the relative positions of the fine energy structure. As the energies of both the pump (800 nm = 12,500 cm^{-1}) and THz probe (0.2 - 2 THz = 7 - 67 cm^{-1}) beams were known, the best ions could be identified by looking for systems that had the top levels of an excited Stark multiplet around 12,500 cm^{-1} and transitions within this multiplet around 10 - 60 cm^{-1}. Looking through Kaminskii's catalogues provided 2 ions that exhibited these favorable energy levels when doped into crystalline hosts: Neodymium (Nd^{3+}) and Erbium (Er^{3+}). These were the ions that were

considered and then combined with the chosen hosts to determine which was best suited for these experiments.

To predict the best possible material for TDS and TRTS experiments, calculations were done that estimate absorption dynamics in various crystalline rare earth ion/host combinations. This is done in order to choose an ion-host combination that has the highest likelihood of showing rare earth absorption of both the 800 nm pump beam as well as the THz probe beam. A relatively easy and simple way of quantifying these parameters for initial calculations is to look at the absorption cross sections of the material at both frequencies. The larger the cross section, the more likely the light will interact with the material and the more likely we will be able to see absorbance from our tests. The absorption cross section can be calculated a number of ways, but the easiest method given the kind of data available to us is through the absorption spectra:

$$\sigma = \frac{4\pi * K(\lambda)}{N * \lambda} = \frac{\alpha(\lambda)}{N}$$

Where K is the extinction coefficient, N is the number density of rare earth ions, λ is the wavelength of interest, and α is the absorption coefficient. Using absorption data in the 800 nm and THz range, the absorption cross section can be estimated to determine whether this effect can potentially be detected in the THz-TDS. By comparing the values between ion-host combinations and combining these with the host absorption information, a good educated guess can be made as to which material is best suited for these experiments.

Optical (800 nm) Cross sections:

Using literature values for the absorption coefficient, absorption cross section, and doping concentration, the response of various ion/host systems can be estimated. For Nd in

similar hosts such as YVO_4, $GdVO_4$, and $Sr_5(PO_4)_3F$, ref. [12] reports an average absorption

coefficient of 50 cm^{-1} at 808 nm. The samples tested had a doping concentration of 10^{20}

ions/cm^3, so the cross section was estimated to be about $5*10^{-19}$ cm^2. For Er^{3+} in $KGd(WO_4)_2$,

studies were done at low temperatures (5K) and reported the absorption due to the ion

absorption. Ref. [13] gives an absorption coefficient of 1.5 cm^{-1} for a sample with $N = 1.1*10^{20}$

ions/cm^3, which gives an absorption cross section of $1.36*10^{-20}$ cm^2. Some previous works even

calculated the absorption cross sections explicitly: for Er^{3+} in $KY(WO_4)_2$, the absorption cross

section was reported for 3 different polarization angles [14]. These averaged at around $0.4*10^{-20}$

cm^2 for samples of 0.5% Er^{3+}. Lastly, for Er^{3+} in $CaWO_4$, ref. [15] reports a room temperature

absorbance at 800 nm of 0.3 cm^{-1}. Their samples had a doping level of $N = 4*10^{-19}$ ions/cm^3, so

the corresponding absorption cross section is $7.5*10^{-21}$ cm^2, the lowest of the 4 order-of-

magnitude calculations done. These results are tabulated in Table 1.

Table 1: Calculated optical absorption cross sections for potential rare earth doped crystals.

	Nd:LiNbO$_3$	Er:KGd(WO$_4$)$_2$	Er:KY(WO$_4$)$_2$	Er:CaWO$_4$
Ion σ_{abs} @ 800 nm	$5*10^{-19}$ cm^2	$1.36*10^{-20}$ cm^2	$0.4*10^{-20}$ cm^2	$7.5*10^{-21}$ cm^2

Far-IR (THz) Cross sections:

Few studies of absorption by Stark levels in rare earth doped crystals have been reported

to date. The only studies concerning the transitions between Stark levels in rare earth ions have

come from groups looking to study the magnetic properties of these elements in oxides. Thus, we

use their absorption data to estimate cross sections just to see if detecting these transitions is

feasible and resolvable compared to the optical absorption.

The first material that has been studied in the far-IR region is $DyScO_3$. One study shows the extinction coefficient K at 222 μm is ~1; this corresponds to a frequency of 1.35 THz [1]. Using the size of the unit cell [16], the ion concentration was found to be $1.56*10^{22}$ ions/cm^3.

$$N = \frac{1}{a^3}, \quad \sigma = \frac{4\pi * K(\lambda)}{N * \lambda}$$

This lead to an absorption cross section of $3.6*10^{-20}$ cm^2. The second material that had far-IR data published was another oxide, $TmFeO_3$. This study reported an absorption value of 80 cm^{-1} at 1.3 THz [3]. The ion concentration was found by dividing the number of ions per unit cell by the volume of the unit cell (4 ions per unit cell, with a unit cell side length a = 230 angstroms [17]), which produced a value of N = $1.74*10^{22}$ ions/cm^3.

$$N = \frac{4}{a^3}, \quad \sigma = \frac{\alpha(\lambda)}{N}$$

This allowed for the calculation of the absorption cross section, which had a value of $4.6*10^{-21}$ cm^2. The other study that researched $TmFeO_3$ reported the transmission through a thin sample for a frequency of ~0.6 THz. The equation for transmitted radiation was used to find the absorption:

$$T = e^{-\alpha L} \quad \rightarrow \quad \alpha = \frac{-\ln(T)}{L}$$

Here the transmission was measured to be $10^{-2.5}$ through a sample of thickness .28 mm [2], which lead to an absorption coefficient of 206 cm^{-1}. This was used with the ion density from the previous paper to calculate the absorption cross section: $1.2*10^{-20}$ cm^2. These results are tabulated in Table 2.

Table 2: Calculated THz absorption cross section for potential rare earth doped crystals.

	Komandin (DyScO$_3$)	Kozlov (TmFeO$_3$)	Zhang (TmFeO$_3$)
Ion σ_{abs} @ THz	$3.6*10^{-20}$ cm^2	$1.2*10^{-20}$ cm^2	$4.6*10^{-21}$ cm^2

While these values cannot tell us between the four possible candidates which one is best suited for THz absorption, it does show us that the THz absorption properties for ion-host combination are comparable in strength to the optical absorption. This is a good sign as the optical absorption has been studied extensively, proving it is detectable and provides enough information for analysis. Since these cross sections are similar, these estimates point to a detectable THz response, something that was never guaranteed from the start of the project.

Host Effects:

While the rare earth ions are the focus of this project as well as much of the research literature available, the hosts can have absorption features as well that could affect each material's performance in spectroscopic tests. If the host is highly absorptive in the 800 nm or THz regions, they could obscure the features of the RE ions absorption, making determining if there is intramultiplet transitions much more difficult. The TRTS scheme that determines these properties is shown in Figure 8. As such, a literature search was also done to try to find the absorption properties of the pure host materials so the possibility of this happening is minimized.

Just as with the choice of suitable ions, Kaminskii's handbook Laser Crystals was initially used to find suitable hosts for the rare earth-doped crystal system. As the host's effect on the energy levels of the ion are small, the ones chosen were those that gave the best structure with the previously identified ions (Nd^{3+} and Er^{3+}). There was one associated with Nd^{3+}

(LiNbO$_3$) and three with Er^{3+} (KGd(WO$_4$)$_2$, KY(WO$_4$)$_2$, and CaWO$_4$). After these were

identified, the main host property that was explored was their absorbance in the 800 nm and THz

range without dopants to see if they would allow for the propagation of signal. As previously

stated, the optimal host would have low absorption in these regions so that the signal can easily

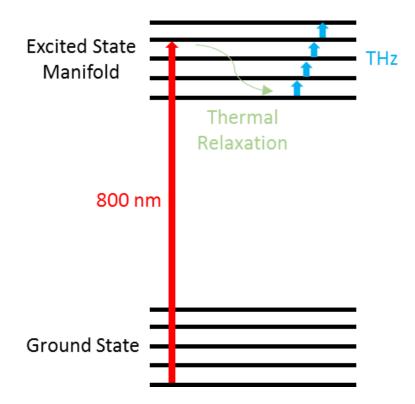pass through and the absorbance from the ion is readily seen.

Figure 8: Simplified diagram showing the basic processes during TRTS of rare earth doped
crystals. The 800 nm pump beam excites ions from the ground multiplet to one of the excited
multiplets, where they begin to thermalize. During this time, THz absorption may be possible,
and this would lead to possible characterization of the excited state dynamics.

For LiNbO$_3$, the absorption edge starts at ~ 354 nm with little to no absorption at energies

below [18]. This implies that the pure host will not absorb the lower energy 800 nm pump beam

as it does not bridge the material's band gap. In the THz range, LiNbO$_3$'s absorption coefficient

increases with frequency [19], with a value of 15 cm^{-1} at 1 THz. This could pose an issue with

resolving the ions THz absorption, but the data shows that the absorption coefficient is different for different polarizations, so by changing the polarization of the probe a clearer signal could be possible.

As many of these materials were studied before reliable far-IR measurements were possible, finding their absorption in the THz range was sometimes difficult. While DFT calculations predict close to zero absorption at 800nm [20], no data about the materials interaction with low energy photons could be found. The only reported dynamics reported were the existence of 'zone-boundary acoustic phonons' at 1.5 - 3 THz [21], but these should not couple with the optical pump beam as they are purely acoustic modes. Thus at this time we do not know how this host absorbs in the far-IR region.

$KY(WO_4)_2$ has been studied in both the optical and THz regions. Ref. [22] shows that below 100 cm^{-1} the system shows < 10% absorbance, which is promising as host phonon modes can occur in this region and lead to high absorption. Unfortunately they do not report the sample thickness, and thus the absorption coefficient could not be calculated. They also report almost 0 absorption at 800 nm, meaning the host likely has no electronic transitions that could interfere with signal transmission. While this seems positive for using this host, two other experiments reported both transmittance and sample thickness, which allowed for the calculation of the absorption coefficient alpha for 800 nm radiation. These two studies ([23] [24]) gave coefficients that agreed well, with the calculated alphas being 2.6 cm^{-1} and 2.9 cm^{-1} respectively. These do suggest that even with no host resonances apparent, there is still significant absorption of the optical beam in this host choice.

$KGd(WO_4)_2$ shows promising figures in the THz range, with low absorbance reported for a sample of $Eu:KGd(WO_4)_2$ [25] and no absorption other than rare earth lines in $Dy:KGd(WO_4)_2$

[26]. Again, calculations for absorption edge were one of the only reliable reported data in the optical region, with an edge at 291nm reported for this material, implying low absorbance of the lower wavelength pump beam present in our setup [27]. While another study shows the absorbance for a sample of $Nd:KGd(WO_4)_2$, there are ionic absorption lines that obscure the intrinsic host absorption. But without these lines it seems like there is very little absorbance, which backs up the absorption edge assumptions from the previous study and makes a stronger case for this host.

While $CaWO_4$ was also identified, the low values for absorption cross section and lack of THz data lead to the other compounds being prioritized. From this analysis and considering the location of the possible energy levels from the literature, it seems that $KGd(WO_4)_2$ is the most promising candidate at this time. It has been used with both Er^{3+} and Nd^{3+} and shows promising transparency in both the 800 nm and THz regions. If this setup is to be used to characterize a crystalline sample, this is the one that would be best suited out of all the ones considered.

Recommendations for 520nm:

After doing calculations with values typical of some of our available Er-doped samples, it was found that the 800 nm absorption line available in our Pump-Probe setup does not sufficiently pump the ions to the point where an appreciable fraction are in an excited state (see pumping fraction calculation section). Because of this, measuring the absorption from this state seems less likely. Even though we cannot change our setup, we would like to present some other ion-host combinations that are active around the highest optical absorption resonance in Er^{3+}: 520 nm (19230 cm^{-1}). These were also found from Kaminskii's <u>Laser crystals</u>, and may be useful for those with access to a tunable pump who want the best chance of seeing excited state absorption in these kind of materials:

Nd in $GdAlO_3$, Nd in $KY(MoO_4)_2$, Er in $CaWO_4$, Er in $YAlO_3$

These materials have an excited manifold with an upper state around the 520 nm energy, which means they are candidates for excitation. These may exist more suitable ion-host combinations with resonances outside of the 800 nm or 520 nm ones presented here, but they would have to be considered separately and as such were not a part of this project at this time.

Pumping Fraction Estimation

To anticipate the material response to TRTS, a preliminary calculation of how many rare earth atoms can possibly be excited by the pump beam would be helpful. Once this calculation is complete, more exploratory calculations will be done by varying the parameters of the excitation beam to see what kind of excitation is best suited for exciting the highest possible fraction of the rare earth ions. We believe that having the highest fraction will allow for the greatest chance of detecting the effects of excited state absorption. To begin, some parameters from one of the silicate samples provided by Prof. Quimby (LG22) were used as well as some figures that represent the THz setup at WPI. These were used to construct the initial calculation.

First, the total amount of pump beam energy absorbed by the sample must be found. This is done using Beer's Law to relate the change in intensity (I) through the sample to the doping concentration of rare earth ions (N_0), the absorption cross section of the ions (σ_{abs}), and the thickness of the sample (z) :

$$I(z) = I_0 e^{-N_0 * \sigma_{abs} * z}, \qquad 1 - \frac{I}{I_0} = Fraction\ Absorbed = \eta$$

By taking the ratio I/I_0, we can find the fraction of light absorbed through the sample (η). This will be used when the number of photons in the pump pulse is known to determine the amount of

photons absorbed by the sample. To start finding this parameter, the fluence (F) of the pump

pulse must be calculated. This can be done using the energy contained within the pulse (E_p) and

the size of the aperture ($\pi(r^2)$) it is passing through as it enters the sample:

$$Fluence = F = \frac{E_p}{\pi(r^2)}$$

The fluence allows us to calculate the photon flux, which represents the number of photons per

unit area passing through the aperture and sample. This is easily calculated when the energy of

the pump beam photons (hv) is known:

$$Photon\ Flux = \Phi_p = \frac{F}{h\nu}$$

Now we can use the fraction of light absorbed with this value to calculate how many photons are

actually absorbed per unit area:

$$\Phi_p * \eta = \frac{Photons\ Absorbed}{Area} = \Phi_{abs}$$

And then by dividing by the sample thickness we can estimate the total number of photons that

are absorbed through the entire part of the sample that is illuminated by the pump pulse:

$$\frac{\Phi_{abs}}{z} = \frac{Photons\ Absorbed}{Unit\ Volume} = n_p$$

This assumes that the sample absorbs weakly so the photons absorbed per unit volume is

constant over the length z. Now that we know how many photons are absorbed in a volume, and

therefore how many ions have been promoted to an excited state, we can calculate the fraction of

ions that are excited by comparing this to the number of ions per unit volume in the illuminated

volume:

$$\frac{n_p}{N_0} = Fraction\ of\ Ions\ in\ the\ Excited\ State$$

This value is important because in order to see the effects of the excited state absorption, we must be able to observe a significant change in THz absorption when comparing the pumped and unpumped sample. This requires an appreciable fraction of ions in the excited state.

800nm Pump:

The first calculation was done based on the silicate sample with the highest doping concentration on hand with the 800nm pump present in the THz lab. The sample has a thickness of z = 5mm, doping concentration N = $2.46*10^{20}$ cm^{-3}, and absorption cross section σ_{abs} = $3.6*10^{-22}$ cm^2 [4]. The optical pump setup has pump pulse energy E_p = .002 mJ, aperture radius r = .075 cm, and pump frequency ν = $3.75*10^{14}$ s^{-1}. Plugging in these parameters into the procedure enumerated above gives a value of .043 for the fraction of intensity absorbed and $3.92*10^{13}$ excited ions per volume, which leads to a fraction excited of $1.59*10^{-7}$. This is not ideal as a significant portion of the atoms would need to be excited in order to see the excited state absorption spectrum in addition to the ground state absorption spectrum.

520nm Pump:

After the first calculation did not show promising results, we needed to explore what kind of parameter changes would lead to better values for the excited fraction and thus a better likelihood that excited state spectra would be detected. The Er doped into the silicate has its highest strength optical absorption at 520nm, so by using the absorption cross section found in the optical tests (σ_{abs} = $1.71*10^{-20}$ cm^2), we can see if changing the pump to 520 nm (ν = $5.77*10^{14}$ s-1), would lead to a better value for the excited fraction. Using this wavelength with the previous calculation method increases the fraction of pump energy absorbed to .878, but only

raises the excited fraction to $2*10^{-6}$, not enough to make the excited state signal any more easily detectable over the ground state.

Required Fluences:

Another parameter that can be changed to try to increase the excited fraction is the pulse energy. If more photons are able to be absorbed the chance of seeing the excited state signal should become higher. The above equations were manipulated and one was made for each wavelength such that they are scalable by the energy per pulse. The algebra done to produce these is shown below. This modification is done to see what energy is needed for a certain fraction of the ions to be pumped to an excited state:

$$\frac{n_p}{N_0} = \frac{(1 - I/I_0)E_p}{\pi r^2 hvzN} = Constant * E_p$$

Fraction Excited (800 nm) = (.0796)E_p

Fraction Excited (520 nm) = (1.057)E_p

These equations show that 520 nm is much more plausible for experimental testing as it would only take 9.5 mJ for 1% absorption, compared to 126 mJ for 800 nm. This is because concentrating that amount of energy in a short time and small space could lead to many effects that skew the data or could even potentially damage the sample.

Occupation and Absorption Simulation

In order to try to predict the THz absorption expected from RE-doped crystal systems, MatLab was used to simulate the populations of the fine energy levels in rare earth ions doped into a crystal lattice. First, there is a thermal distribution within the ground manifold that must be

first accounted for since tests would be done at room temperature (T ~ 300K), from which the steady state absorption of the ground state can be calculated. This can be done without modeling absorption dynamics because the transitions induced by the probe beam are negligible compared to the thermal populations. This gives as a representation of what we should see in initial TDS spectroscopy experiments. After this, a pump will be introduced to model TRTS, which will excite some of the electrons to the top of a higher energy manifold. As they relax, the absorption spectrum will change on the picosecond timescale; this is what the second section of the simulation intends to model. This excited state absorption profile will be compared to the initial simulation of the ground state absorption to determine what changes we would see in THz measurements if absorption from the excited state in addition to the ground state was observed.

PART 1: First, we simulate the ground state absorption by taking into account the thermal distribution, as our tests will be at room temperature. We can assume an average occupation will be sufficient and use the knowledge of the energy level positions in the material to calculate the expected occupation of each hyperfine level using Boltzmann statistics.

$$\langle N_i \rangle = \frac{N}{Z} g_i e^{\frac{-E_i}{kT}}, \qquad Z = \sum_i g_i e^{\frac{-E_i}{kT}}$$

Here N represents the population of each level, E_i represents the energy of each state, g_i is the degeneracy of each state, T is the temperature of the system, and Z is the partition function that describes the energy structure of the whole multiplet. The degeneracy here is assumed to be 1 for each state for simplicity, but these conditions can be easily changed for Kramers-Degenerate ions or other systems with degeneracy. The model was based around Er in $CaWO_4$. With the basic concepts laid out, the MatLab code will now be presented in sections to show how the simulation was made and what each part does:

```
index = 1:1:7;
%Denotes # of Levels of Interest

N = 10^20;
%Ion Density (cm-3)

Eb = [0;19;25;61;228;266;319];
%Location of Energy Levels (cm-1)

k = 1.38e-23;
%Boltzmann Constant

T = 300;
%Lab Termperature (K)

g = ones(length(index), 1);
%Degeneracy of Each State
%Multiply by 2 for Kramers Degenerate

Z_ = zeros(length(index), 1);
%Vector for Z: Partition Function
```

This first section of the code sets up the main parameters needed to create the Boltzmann distribution. The index parameter denotes how many energy levels there are in the ground multiplet and scales the upcoming vectors to that size accordingly. The N parameter represents the total doping density of the rare earth ions, which will be divided among the levels depending on the temperature. The Eb vector, which stands for 'Energies - Boltzmann' to distinguish it from any following energy level vectors, is a vector with the same length as the index parameter denoting the individual energy level positions in cm^{-1} (all unit conversions will be made while the equations are being processed). Then some necessary values such as the Boltzmann constant, the temperature the spectroscopy measurements will be done at, and the degeneracy of each state are quickly defined. Finally, a 'blank' vector (at this point containing only 1's) is created for the partition function Z, represented by Z_. This will be populated using a for loop in the next section.

```
for i = 1:length(index)
    g_i = g(i);
    Eb_i = (1.986e-23)*Eb(i);
    Z_i = g_i * exp(-Eb_i/(k*T));
    Z_(i) = Z_i;
end

Z = sum(Z_);

for i = 1:length(index)
    g_i = g(i);
    Eb_i = (1.986e-23)*Eb(i);
    N_(i) = (N/Z)*g_i*exp(-Eb_i/(k*T));
end
```
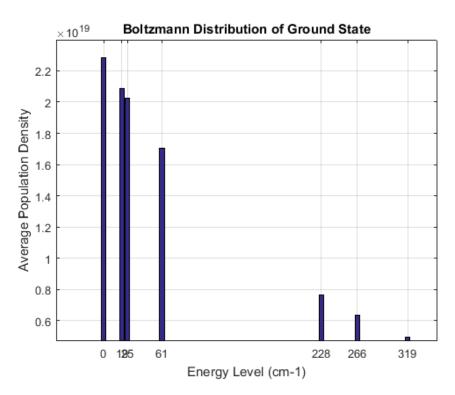

Figure 9: Example chart for Boltzmann distribution of the ground multiplet.

The first for loop above, which directly follows the establishment of the Z_ vector, populates said vector with individual values of the partition function, each one corresponding to a particular energy level from the Eb vector. The population follows the partition function

equation closely; the only difference being a conversion of the energy levels from cm^{-1} to Joules to match the kT term it will be divided by. After the for loop populates the Z_ vector with elements for each energy, they must be summed to get the functional value for Z. This is done with a simple sum command. To calculate the thermalized population in each state, one more for loop must be executed corresponding to the first equation shown in the beginning of this section. This follows similar steps as the for loop for the partition function, but uses this result and the total doping concentration N to output the occupation of each state N_. This is then plotted to show the expected relationship between energy and occupation, shown in Figure 9.

The absorption spectrum can be easily calculated once the occupation (N) of each level is known by using the absorption cross section (σ) of each state. This equation represents the absorption of radiation with energy equal to the difference between the starting level to the excited level:

$$\alpha(\omega_{1\rightarrow2}) = N_1(\omega_{1\rightarrow2}) * \sigma(\omega_{1\rightarrow2}) - N_2(\omega_{2\rightarrow1}) * \sigma(\omega_{2\rightarrow1})$$

As the transition rates induced by the absorption of the THz pulse are an order of magnitude smaller than the nonradiative rates between Stark levels, we do not have to model the populations caused by probe beam absorption, only the absorption expected from the already calculated thermal distribution. Also, only one σ value is needed since for two states i and j, $\sigma_{ij} = \sigma_{ji}$. Once calculated, these α values can be used in Beer's Law with the thickness of the sample to calculate the expected difference in intensity from the incident beam and the transmitted beam and can be compared to the absorption spectrum of the excited state to pick out differences that would denote excited state absorption.

```
% Create the Sigma Matrix
P=zeros(7,7);
P(1,:) = [0 2 4 3 5 9 8];
P(2,:) = [2 0 4 5 6 6 5];
P(3,:) = [4 4 0 7 6 8 4];
P(4,:) = [3 5 7 0 4 6 9];
P(5,:) = [5 6 6 4 0 3 2];
P(6,:) = [9 6 8 6 3 0 4];
P(7,:) = [8 5 4 9 2 4 0];
sigma=(P).*(1e-20*ones(7,7));


% Planck's Constant
h = 6.626e-34;

% Double Sum Alpha
for j=1:7;
    for i = 1:7;
        alphab(i,j)=sigma(i,j)*N_(i)-sigma(j,i)*N_(j);

    end
end

% Restructure Alpha Matrix
alphab = alphab(:,2:7);
alphab = alphab(1:6,:);
alphab(3:6,1)=0;
alphab(4:6,2)=0;
alphab(5:6,3)=0;
alphab(6,4)=0;
```

To accomplish this, an n by n matrix is first created with n = length(index) to represent all the σ values needed. The matrix is symmetric since $\sigma_{ij} = \sigma_{ji}$, and the elements are then multiplied by 10^{-20} to match the order of magnitude expected from the papers found through literature review. Since little is known about the absorption cross section other than its order of magnitude, random integers were assigned in the σ matrix, and can be changed to see how this affects the absorption spectrum. Actually evaluating α requires a double sum, and therefore a double for loop. This performs the calculation of the above equation for every value of i and j, which counts each transition twice since the ij and ji transitions are both considered in the ij case of the sum. Therefore, we must remove the superfluous values from the absorption data before plotting and

analyzing. This is simply done by restructuring the resultant n by n α matrix to be upper

diagonal; here this is accomplished by setting all the lower diagonal values manually to zero.

Now that we have an absorption value for each transition, we need to know what frequency these

correspond to.

```
% Double Sum Nu
for j=1:7
    for i = 1:7
        nub(i,j)=(1.986e-23)*(abs(Eb(j)-Eb(i)))/h;
    end
end

% Restructure Nu Matrix
nub = nub(:,2:7);
nub = nub(1:6,:);
nub(3:6,1)=0;
nub(4:6,2)=0;
nub(5:6,3)=0;
nub(6,4)=0;

ALPHAb = reshape(alphab,[36,1]);
NUb = reshape(nub,[36,1]);
```

In a similar fashion, we create an n by n matrix where each element is the difference in

energy between the ith and j^{th} state (abs() function guarantees the energy difference is positive);

this is done by another double sum represented as a double for loop. Here the 'nub' matrix stands

for 'Nu Boltzmann' to separate it from following frequency matrices. This matrix is structured

exactly the same as the previous α matrix to remove overlapping values to guarantee a one-to-

one correspondence between the two matrices. Now the α and ν matrices are both converted into

column vectors using the reshape command so ordered pairs can be made from their elements for

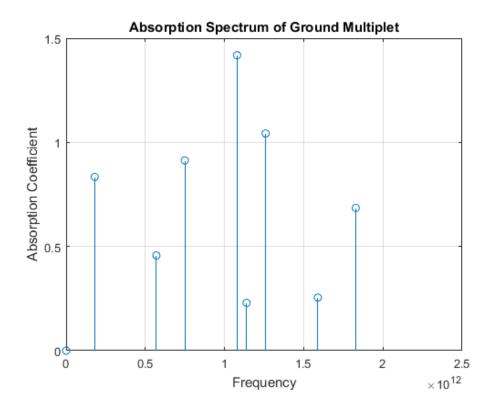plotting. This 'point plot' for absorption is shown in Figure 10.

Figure 10: Absorption coefficient as a function of frequency for the ground multiplet at room temperature.

After the individual absorption peaks have been found and plotted, the effects of temperature and other broadening much be taken into account. This is done by applying Lorentzian peaks to the absorption features, which can then be continuously summed over to create an absorption spectrum containing the broadened contributions from all of the peaks. The equation for a Lorentzian distribution is as follows:

$$L(x) = \frac{1}{\pi} \frac{\frac{1}{2}\Gamma}{(x - x_0)^2 + (\frac{1}{2}\Gamma)^2}$$

Where x_0 represents the center point of the distribution and Γ is a parameter specifying the width of the distribution. The function is normalized to the peak value by multiplying the function by a

constant factor of $\pi\Gamma/2$, as the values for σ already account for the response of a broadened feature. These functions are applied in the code as follows:

```
gamma = (2e12).*ones(length(ALPHAb), 1);
x = 0:1e10:10e12;

for i = 1:length(NUb)
    Lorentz(i,:) = 1/pi*(0.5*gamma(i))./((x-NUb(i)).^2+(0.5*gamma(i))^2);
end

for i = 1:length(ALPHAb)
    ScaledLorentz(i,:) = Lorentz(i,:)*ALPHAb(i)*((1/2)*(pi)*(gamma(i)));
End
%Extra scaling factor normalizes at max, then ALPHAb scales
```
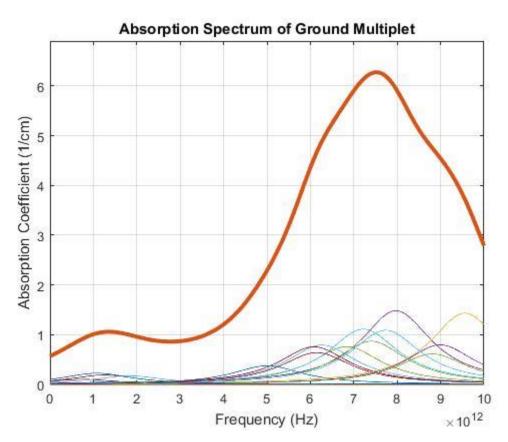

Figure 11: Absorption spectrum of the ground state calculated by summing Lorentzian peaks applied to each absorption feature. The system used was Er in $CaWO_4$ with a doping concentration of 10^{20} ions/cm^3.

With these functions applied, the Lorenztians are summed and then plotted on the original frequency scale set by the NUb vector, producing a final plot of the absorption spectrum of the ground state. This plot is shown in Figure 11. The individual peaks are shown with thin lines, whereas the sum over all Lorentzians is shown with a bold line. This spectrum models the response of the unexcited rare earth ions in TDS measurements.

PART 2: The second part of the simulation is concerned with the transient absorption due to an optical pump. This pump will excite a fraction of the electrons from the ground manifold to the top of an excited manifold (a material with energy levels that satisfy this condition is chosen such that this occurs). They will then relax down through the manifold by emitting phonons, before settling back to the lowest excited manifold state and eventually down further to a lower manifold.

```
N_initial = [0;0;0;0;0;10^20];
% Original Occupation Density Values

Wup = [(1)*10^12; (2)*10^12; (1)*10^12; (2)*10^12; (3)*10^12; (4)*10^12];
% Rate Values (1/tau)
% First element represents ground state, which was omitted from this run

% Define Energy Level Structure (cm-1)
E = [12190;12323;12355;12374;12451];

n = [
    1;
    1;
    (1/(exp((1.986e-23)*(abs(E(2)-E(1)))/(k*T))-1));
    (1/(exp((1.986e-23)*(abs(E(3)-E(2)))/(k*T))-1));
    (1/(exp((1.986e-23)*(abs(E(4)-E(3)))/(k*T))-1));
    (1/(exp((1.986e-23)*(abs(E(5)-E(4)))/(k*T))-1))
     ];
% Set boltzmann-like factor for each transition
% n = 1/(e^(hw/kT)-1)
% Lowest state has ~0.1 ms lifetime, so set n = 1 here and fix in Wdown

Wdown = [
    (2)*10^4;
    (2)*10^4*((1+n(1))/n(1));
```

```
    (1)*10^12*((1+n(2))/n(2));
    (2)*10^12*((1+n(3))/n(3));
    (3)*10^12*((1+n(4))/n(4));
    (4)*10^12*((1+n(5))/n(5))
        ];
% Thermalization Rate Values [Wdown = Wup*((1+n)/n)]

initial_conditions = N_initial;
% Define the Intitial Conditions vector

time_initial = 0;
time_final = 10^-11;
time_step = 5e-15;
time_stamp = time_initial:time_step:time_final;
% Define the Time Span

[t_case, x_case] =  ode45(@(t,x) Dringoli_Integration(t, x, W,
N_initial),time_stamp,initial_conditions);
```

This section of the code begins similarly with defining vectors containing key values for the eventual rate equation simulation. N_initial represents the initial occupation of the ground state and each states within the excited manifold. The ion used in this example has 5 excited states, so this vector has 6 elements adding the ground state. The uppermost state is the one being pumped too, so its initial state should be equal to the amount of ions excited by the pump beam. In this case this value is highly exaggerated (10^{20} excited atoms per unit volume) to show the effects on a visible scale. The next vectors needed represent the relaxation rates of each excited state. There is not much data available for these values, but in general these systems relax on the picosecond timescale, so they are set as such, with the relation between relaxation time (τ) and the rates (W) being:

$$W_i^{up} = \frac{1}{\tau_i}, \quad W_i^{down} = W_i^{up}\left(\frac{n+1}{n}\right), \quad n = \frac{1}{e^{h\omega/2\pi kT} - 1}$$

In order to accurately model both the absorption and relaxation transitions, two W vectors must be defined for each direction, Wup and Wdown. Wdown has an additional dependence on temperature and the difference in energy as these are the parameters that affect thermalization, which is contained in the parameter n. Next comes the setup for solving the rate equation, which just defines the initial conditions as the starting populations and the timespan/timesteps. Since the relaxation phenomena happen in picoseconds, 10 picoseconds was chosen as an appropriate timescale, but it can be modified depending on the speed of the processes one wants to observe. The relaxation itself is governed by one coupled equation for the population of each state, which takes into account both nonradiative transitions (first two terms) and THz absorption (second two terms):

$$\frac{dN_j}{dt} = N_{j+1}W_{j+1}^{down} - N_j W_j^{down} + N_{j-1}W_j^{up} - N_j W_{j+1}^{up}$$

Where all instances of N_j represent the population of a particular level and the W's are the rates of the transition. The subscript on the symbol W refers to the upper level of the transition. These are enumerated in their own MatLab file which is called by ODE45 in the main script:

```
function N_state = Dringoli_Integration(t, x, W, N_initial)
% This time = index of current time in the big time stamp array

N0 = x(1);
N1 = x(2);
N2 = x(3);
N3 = x(4);
N4 = x(5);
N5 = x(6);

Wu0 = Wup(1);
Wu1 = Wup(2);
Wu2 = Wup(3);
Wu3 = Wup(4);
Wu4 = Wup(5);
```

```
Wu5 = Wup(6);

Wd0 = Wdown(1);
Wd1 = Wdown(2);
Wd2 = Wdown(3);
Wd3 = Wdown(4);
Wd4 = Wdown(5);
Wd5 = Wdown(6);

N0_dot = -N0*Wu0;
N1_dot = N2*Wd2-N1*Wd1-N1*Wu2;
N2_dot = N3*Wd3-N2*Wd2+N1*Wu2-N2*Wu3;
N3_dot = N4*Wd4-N3*Wd3+N2*Wu3-N3*Wu4;
N4_dot = N5*Wd5-N4*Wd4+N3*Wu4-N4*Wu5;
N5_dot = -N5*Wd5+N4*Wu5;

N_state = [N0_dot;N1_dot;N2_dot;N3_dot;N4_dot;N5_dot];
```

This process mainly concerns taking the information already put into the code and turning it into parameters the solver (ODE45) can process. The elements from the N vector are mapped to the x variable, which is what is solved for, and each value from the N, Wup, and Wdown vectors are given a unique tag so they can be represented in the rate equation easily. Then the rate equation in parsed out identically as shown in the equation above, and the derivatives are collected into the N_state vector to be solved. Running the command in the original script and graphing the output gives the population dynamics for the given parameters, shown in Figure 12.

Due to the quasistatic nature of the lowest excited state, the ions do not relax out of the excited multiplet quickly and form a distribution similar to the thermal distribution of the ground state. This distribution is simplified due to the estimated rate values, and should be reconsidered if this simulation is to be compared to TRTS results in the future. After the populations are calculated, an absorption spectrum can be calculated similarly to the ground state:

$$\alpha(\omega_{1 \to 2}) = N_1(\omega_{1 \to 2}) * \sigma(\omega_{1 \to 2}) - N_2(\omega_{2 \to 1}) * \sigma(\omega_{2 \to 1})$$
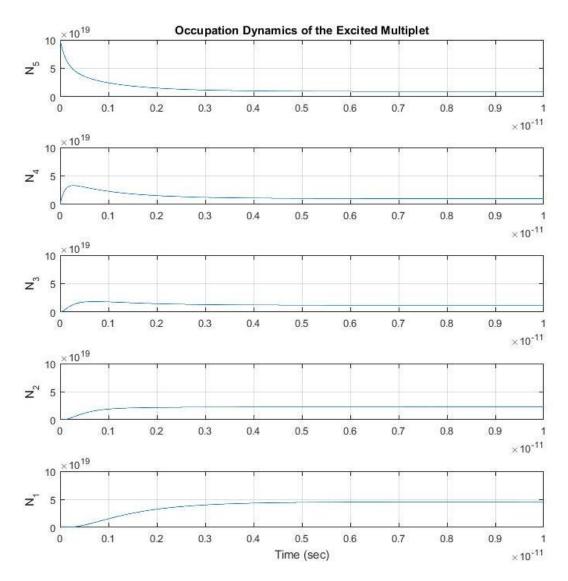
Figure 12: Occupation dynamics of the pumped excited multiplet.

This is done using very similar MatLab operations as well:

```
% Define Energy Level Structure (cm-1)
E = [12190;12323;12355;12374;12451];

% Planck's Constant
h = 6.626e-34;

% First Time Instance
time1 = t_case(5);
state1 = x_case(5,:);
N1=state1(2);
```

```
N2=state1(3);
N3=state1(4);
N4=state1(5);
N5=state1(6);
N=[state1];
```

Here the energy levels of the excited multiplet are enumerated once more. After this, necessary

constants are defined and a time instance is chosen from the rate equation solution. This choice

of time also denotes a particular choice of N for each state, so they are given values and put into

a vector of their own.

```
% Create the Sigma Matrix
P = zeros(5,5);
P(1,:) = [0 9 7 9 8];
P(2,:) = [9 0 6 9 7];
P(3,:) = [7 6 0 9 8];
P(4,:) = [9 9 9 0 6];
P(5,:) = [8 7 8 6 0];
sigma=(P).*(1e-20*ones(5,5));

%Double Sum Alpha
for j=1:5
    for i = 1:5
        alpha(i,j)=sigma(i,j)*N(i)-sigma(j,i)*N(j);
    end
end


% Restructure Alpha Matrix
alpha = alpha(:,2:5);
alpha = alpha(1:4,:);
alpha(3,1)=0;
alpha(4,1)=0;
alpha(4,2)=0;

%Double Sum Nu
for j=1:5
    for i = 1:5
        nu(i,j)=(1.986e-23)*(abs((E(j)-E(i)))/h);
    end
end

%Restructure Nu Matrix
nu = nu(:,2:5);
nu = nu(1:4,:);
nu(3,1)=0;
nu(4,1)=0;
```

```
nu(4,2)=0;

ALPHA = reshape(alpha,[16,1]);
NU = reshape(nu,[16,1]);
```
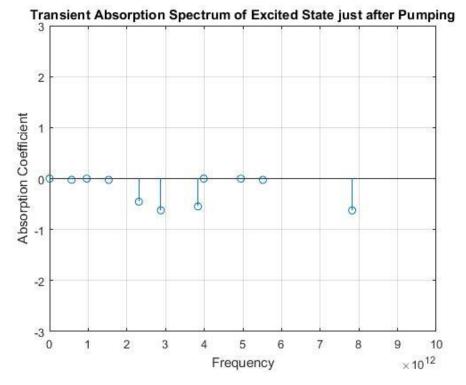

Figure 13: Excited state absorption features just after excitation.

Next, the absorption based on these particular occupation levels are calculated. These are done exactly the same as the previous section, so the details will not be repeated. The main difference is the size of the matrices involved: since the ion used in this example has only 5 states in the excited manifold all the matrices start as 5 by 5. Once all the double sums have been calculated and the restructuring has been completed, the absorption can be plotted. The result, another point plot, is shown in Figure 13.

Just as with the ground state calculations, the peaks must be broadened due to differences in the exact positions of the energy levels due to finite temperature, this is done in a very similar fashion:

```
gamma1 = (2e12).*ones(length(ALPHA1), 1);

x = 0:1e10:10e12;

for i = 1:length(NU)
    Lorentz1(i,:) = 1/pi*(0.5*gamma1(i))./((x-NU(i)).^2+(0.5*gamma1(i))^2);
end

for i = 1:length(ALPHA1)
    ScaledLorentz1(i,:) = Lorentz1(i,:)*ALPHA1(i)*((1/2)*(pi)*(gamma1(i)));
End

%Extra scaling factor normalizes at max, then ALPHAb scales
```

This results in a similar spectrum, consisting of the sum over individual absorption features. Since any 'slice' of time in the rate equation simulation can be called, it is possible to see how the absorption spectrum of the excited state changes in time as the ions relax down through the multiplet. This is done by simply changing the parameters 'time' and 'state', which are called early on in the section, then the calculations are repeated exactly. The 'time' parameter takes on integer values determined by the number of timesteps that have taken place. Figure 14 shows an absorption spectrum calculated right after pumping and Figure 15 shows an absorption spectrum calculated for a time corresponding about halfway through the relaxation process.
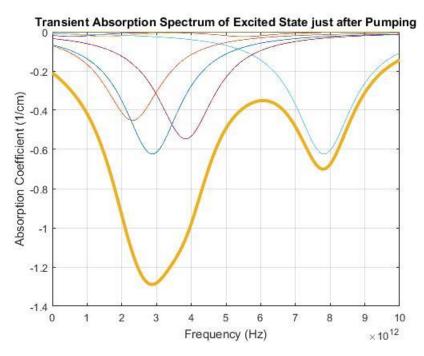
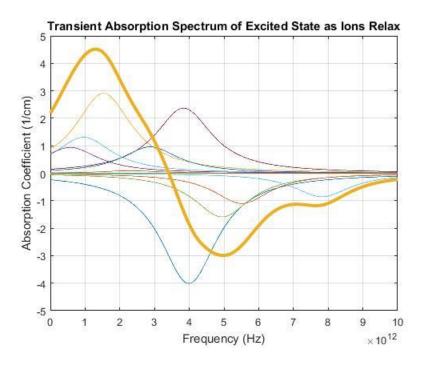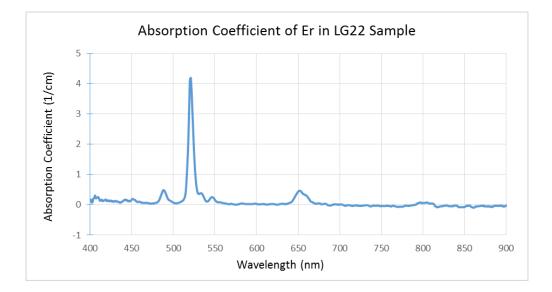Figure 14: Change in absorption due to excited state transitions taken just after excitation.

Figure 15: Change in absorption due to excited state transitions halfway through relaxation. Each thin line represents an individual broadened absorption feature, and the bold line represents the sum of all of all the features.

These plots show that detecting changes in the absorption spectrum are possible, and that these changes can act as a marker for rare earth ion absorption dynamics. Due to the finite occupation of each level, a negative absorption is possible, which corresponds to the stimulated emission of THz photons as ions transition down through the multiplet.

With both the ground multiplet and excited multiplet absorption spectra calculated, they can be compared for different times in the excited state relaxation process to see what specific signatures would be detected, if the THz spectroscopy experiments are picking up transitions within the excited state, and for what time delays between pump and probe we expect to see these features. This will be helpful as these estimates can be compared to experimental data to see if the results of experiments are consistent with the absorption dynamics we expect from these type of systems given the doping concentration and other properties within the sample.

Experimental

While the main focus of the experimental section of this project is identifying spectroscopic signatures of intramultiplet absorption in the THz range, it is necessary to start with optical spectroscopy in order to establish the rare earth concentration of each sample from optical absorption. The measured doping concentrations can then be used to estimate the expected THz intramultiplet absorption. We will also look for a correlation between optical absorption of the rare earth ion and THz absorption, which would support the hypothesis that the THz absorption is caused by absorption of the rare earth ions.

Optical Spectroscopy

Figure 16: Absorption spectrum of Er found through optical spectroscopy of the homogeneous silica sample LG22, showing the absorption peak at 520 nm.

Er is known to have a strong optical response at 520 nm due to transitions within its 4f electron shell, which are dipole-allowed in the case of broken inversion symmetry and are also

available through a high degree of admixing of other states. This is shown in Figure 16. The core-cladding samples used were the precursors of optical fibers, and therefore had an Er-doped core and non-doped cladding, allowing us to make measurements with and without rare earth-doping. Each core reported a different level of doping that would be found through these tests. In addition, we looked at other silica samples with a homogeneous distribution of rare earth ions. The difference in the two homogeneous samples was the doping concentration, which was a factor of 100 higher in the second sample of the set (LG22). By choosing the most resonant peak in the Er optical absorption profile (520 nm), the optical absorption data was well resolved and required only a small tabletop setup, which will be explained below.

Figure 17: Core/cladding sample showing the difference between the undoped outside region and doped core (spot in the center showing reflection).
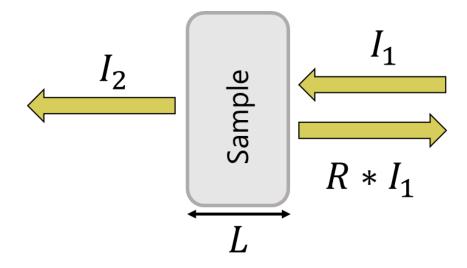
Figure 18: Simple diagram showing the basic parameters considered in the optical spectroscopy tests. Reflection can be corrected for, and then the difference in intensities can be correlated to the absorption or doping concentration.

The UV-Vis spectroscopy setup consists of a halogen bulb placed at the far right with a small aperture next to it to create a small shaft of light for testing. Each glass sample was prepared by making a foil mask with a small hole about the size of the halogen light and placing it on the part of the sample we wanted to analyze (this was especially important for the cladding-core samples, shown in Figure 17). After the light passed through the sample, it was collected by placing an optical fiber close to the exiting light. A basic diagram of this setup is shown in Figure 18. This light was fed through a pocket spectrometer for spectroscopic data acquisition. For each sample, the dark spectrum of the detector (response when no signal is input), bulb spectrum, and sample spectrum were taken (For cladding/core samples individual measurements were made for the cladding vs. the core).

Acquiring the dark spectrum of the detector, the lamp spectrum, and finally the spectrum of light passing through the sample will allow us to calculate the absorption coefficient. From these the doping concentration (N) can be found and used to evaluate the results of future THz

measurements on the ground state absorption. Applying Beer's Law allows for the direct calculation of the absorption coefficient:

$$I_2 = I_1 * (1 - R) * e^{-\alpha L}$$

Solving for α gives:

$$\alpha = \frac{\ln(1 - R)}{L} + \frac{\ln(I_1/I_2)}{L}$$

Data analysis was done using Excel, with the left reflection term removed by fitting a trendline to the background data and subtracting it to get an accurate value for the absorption peak due to the rare earth ion doping. The absorption coefficient alpha was used in the equation:

$$\alpha = \sigma * N$$

This can be used to find σ if N is known and vice versa (depending what was known initially). This way N could be found and compared to the results of THz experiments. This calculation also can act as a check, as the computed N value could be compared to a known value (if available) to confirm the validity of the optical tests.

UV-Vis spectroscopy allowed for the determination of the doping concentration so that the THz measurements can be correlated to the absorption of the rare earth ions. An example spectrum (the core of one of the core/cladding samples) and its processing are provided below; the rest of the data for the other samples will be tabulated and discussed after.

To start, the total signal change due to both reflection losses and sample absorption was plotted. This is shown in Figure 19.
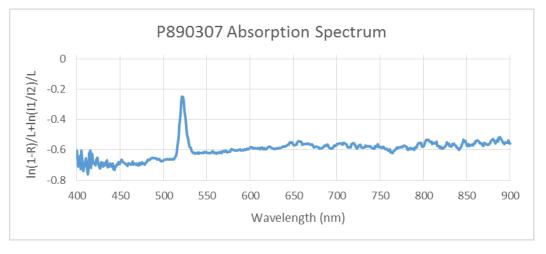
Figure 19: Unprocessed absorption data of P890307 represented by $\alpha = \frac{\ln(R-1)}{L} + \frac{\ln(I_1/I_2)}{L}$

Then a section of the background data (represents non-rare earth losses such as reflection, transmission, and host absorption) was isolated and fit with a simple trendline, shown in Figure 20.
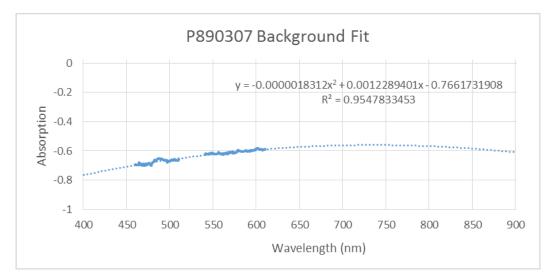

Figure 20: Fitting non-rare earth losses in P890307.

After this, the trendline function was plotted on its own so that it could be subtracted from the main loss data. Finally, the trendline was subtracted from the main data to remove the reflection component, leaving only the absorption from within the sample. This is shown in Figure 21.
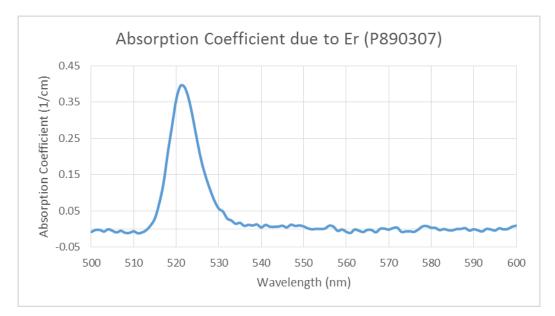
Figure 21: Losses only due to rare earth absorption in P890307; represents α.

The peak of this absorption feature was taken to be α, which could then be compared to others and/or used to calculate N or σ. The results are tabulated in Tables 3 and 4, with the first set being the cladding/core samples and the second set being the homogeneous samples (N values were found from material specification sheet and confirmed):

Table 3: Core/cladding samples optical test results, where known σ and experimentally found α were used to calculate N for each sample.

	α	σ	N
P890307	0.4 1/cm	$2.9*10^{-20}$ cm^2	$1.38*10^{19}$ ions/cm^3
P881027	0.34 1/cm	$2.9*10^{-20}$ cm^2	$1.17*10^{19}$ ions/cm^3
P880608	0.15 1/cm	$2.9*10^{-20}$ cm^2	$5.17*10^{18}$ ions/cm^3

Table 4: Homogeneous samples optical test results, confirming that the doping level differs by a factor of ~100.

	α	σ	N
LG20	0.05 1/cm	$1.7*10^{-20}$ cm^2	$2.69*10^{18}$ ions/cm^3
LG22	4.2 1/cm	$1.7*10^{-20}$ cm^2	$2.46*10^{20}$ ions/cm^3

This test will allow us to compare the THz measurements directly to doping concentration, and also allowed us to confirm that the difference in doping between the two homogeneous samples was ~ 100.

THz Spectroscopy

We have carried out THz-TDS measurements for all samples, testing many different doping concentrations. This is done hoping to see that a higher doping concentration leads to higher THz absorption which would present good first evidence of THz absorption directly between multiplet levels in these materials.
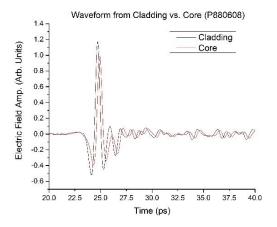
For the core/cladding samples, waveforms were taken for air (with no sample for reference), for the cladding, and finally for the core. These measurements in the time domain were transformed to the frequency domain through a FFT so that the absorption as a function of frequency could be analyzed. The cladding and core measurements for the same sample were first compared to see if any difference could be seen due to the presence of Er in the core but not the cladding. Then different samples were compared to see if the different doping concentration had any effect on the THz signal. Finally, the THz absorbance was calculated by comparing the difference in frequency components between the cladding and core spectra.

The pure silica samples were analyzed the same way, but without separate measurements for the cladding and core since each sample was homogeneous. These tests also acted as checks to reduce the effects of any possible artifacts from slightly different hosts/geometries (reflections from core/cladding structure, etc.). These samples also had a higher difference in doping concentration, which was confirmed by optical tests, so ideally they would show a more distinct difference in absorption.

In the analysis of these samples, some consideration must be given to the assumptions made in the analysis. Typical samples tested with this particular THz setup are thin, largely deposited films on a transparent substrate. In contrast, the core/cladding and homogeneous samples are considered thick, in that the transit time of the THz pulse through the sample is significantly larger than the pulse duration [28]. This causes the reflections that come from the pulse oscillating within the sample to be resolvable in time. These reflections can be individually considered if the refractive index or absorption needs two equations in order to resolve any uncertainty in these parameters. These thick samples also delay the pulse significantly, this must be considered when determining the scan parameters. As this project is not particularly concerned with determining index of refraction, this does not need to be heavily considered, but it is useful to make note of the differences, especially when using software to calculate absorption that is optimized with thin-film approximations. In the future, considering the unique dynamics of absorption in optically thick samples may be able to remove some uncertainty from THz spectroscopy measurements of these kind of samples once the differences are understood.

Figure 22 shows the THz pulses transmitted through the core as well as cladding of one of the core/cladding samples. There are two main effects that should be noted: the time delay and attenuation. Since the thickness is constant across the core and cladding, the time delay results from differences in the refractive index. We are more interested in the second difference, as the attenuation can be processed to see what frequencies are being absorbed and by how much. This is better seen by Fourier transforming the temporal data into frequency space, allowing us to see what frequencies are absorbed and therefore calculate relative absorption. This is shown in Figure 23. These can be compared across samples of different doping concentrations to try to find a correlation between doping concentration and absorption.

Figure 22: P880608 time-domian waveforms for both the cladding and the core.

Figure 23: P880608 FFT spectra showing frequencies within each transmitted pulse.

Looking specifically at the data presented above, the pulse from the core is delayed slightly, marking a definite difference in refractive index at the THz frequencies. As there is a difference in refractive index, changes in reflection must be accounted for. Calculations of the reflection coefficient were done and it was shown that the field reflection coefficient only changed by a maximum of 0.003, which could not account for the difference in electric field magnitude seen by the tests. Thus, losses from reflection were considered negligible for these experiments.

In addition to the delay, the frequency spectrum is diminished around 1 THz, meaning that absorption in the core is higher than this of the cladding. There are a few possible reasons for this difference, the rare earth ions, differences in the host composition between the cladding and core, and differences in reflection. This kind of effect was seen in all three cladding/core samples, and when the absorption is calculated and plotted there is a noticeable trend, shown in Figure 24.
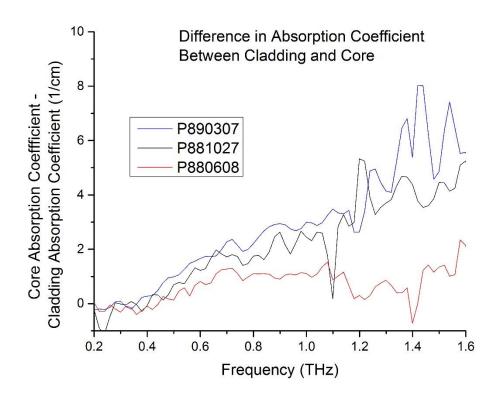
Figure 24: Difference in absorption coefficient of each core compared to its cladding.

While the data is quite noisy, it seems that the samples' absorption coefficients have scaled with their doping concentration. P890307 and P881027 have similar concentrations, with the former having slightly more, and P880608 has significantly less. This behavior is directly mirrored by the measured absorption (particularly in the 1.2 – 1.7 THz region). While it seems like these results point to the rare earth concentration causing the absorption, there are some other differences between the samples that must be considered as confounders. To see if these confounders play a significant role or if the absorption features are accurate to what is expected of these transitions, an iteration of the ground state simulation was also run with the values of each core sample doping concentration, shown in Figure 25. While the curves seems to follow the same trend, the expected absorption is 1 to 2 orders of magnitude below what is seen in

experiment, suggesting additional features are the main source of the absorption signature seen in the core samples.
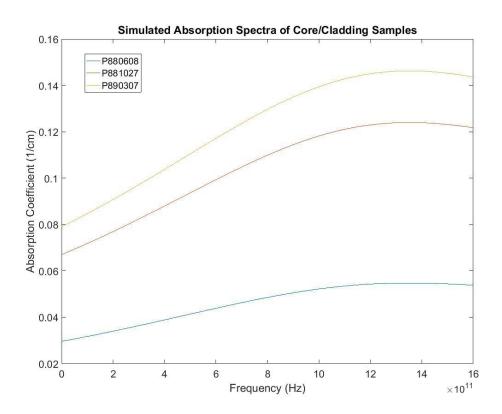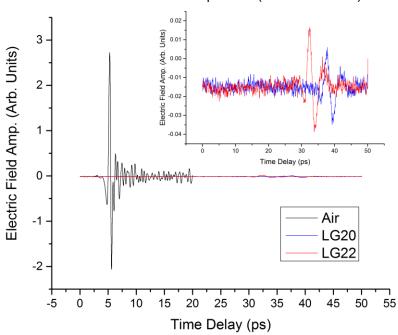

Figure 25: Ground state absorption spectra simulation for doping concentrations present in the cores of the core/cladding samples. Note that the expected absorption is 1 to 2 orders of magnitude less than what is seen experimentally.

As the cores of these samples were designed to become the cores optical fibers, they also contain Al and P in varying amounts. The addition of these elements could possibly change the THz response of the samples, as the Al-O and P-O bonds have different vibrational frequencies, possibly in the THz range. In order to remove this possibility, pure samples of the core host material would have to be investigated to see if these composition differences are the main source of the difference in absorption or if the features can be correlated with the rare earth concentration.

The homogeneous samples had a more pronounced difference in doping concentration, so we expected to see a much more pronounced difference in the absorption signatures as a result. Unfortunately, the thickness of the samples and the fact that their host had a greater number of codopants meant that the THz probe signal necessary for TDS measurements was heavily attenuated. This effect is shown by the red and blue curves in Figure 26.

Figure 26: Time-domain transmitted waveforms for homogeneous silica samples.

The insert in the image above shows a close-up of the waveforms transmitted though the samples. There was very little signal left, and it was mostly in the very low frequency range (<0.2 THz). Even so, we were able to calculate the absorption of the homogeneous samples the same way as the core/cladding samples, shown in Figure 27.
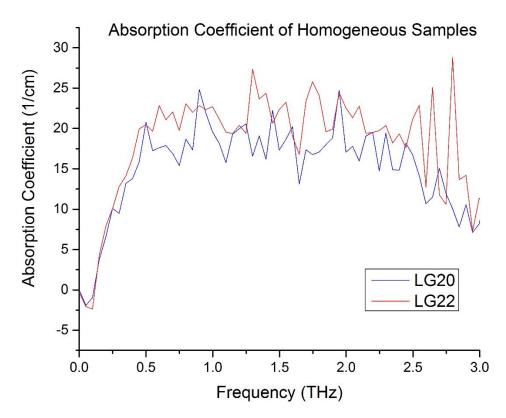
Figure 27: Absorption coefficient of each homogeneous silica sample compared to air.

The absorption present in these samples is higher than in the core/cladding samples as expected, due to the greater number of codopants such as Al, Ca, Li, and Na. But the difference between the two samples (which would be attributed to rare earth absorption) is barely distinguishable through the noise, even though the higher doped sample (LG22) does show the nominally higher absorbance. This leads us to believe that the host effects dominated absorption in this case, and therefore these results cannot be correlated directly to the level of rare earth doping as well.

Conclusions

Over the course of this project, a number of methods have been used to try to anticipate the usefulness and feasibility of THz spectroscopy methods for the investigation of rare earth doped crystal systems. Simulations and calculations were performed in order to anticipate the response of the material systems and find methods of approach that give the best chance of measuring the dynamics of interest. Then, preliminary experiments on glassy samples were done to try to correlate the doping concentration of the materials to the magnitude of THz absorption seen in THz-TDS tests. Finally, a literature search was done in order to find the best candidate rare earth doped crystals for the testing apparatus and methodology presented here.

The simulations done in MatLab show that there exist both ground-state and excited-state absorption features in the THz bandwidth available, and that these features should be resolvable in THz-TDS tests. For excited state TRTS measurements, however, the number of ions that are raised to the excited state are predicted to be too small to produce noticeable transient absorption features, even though there are many possible transitions within the bandwidth. Thus, using a more heavily doped sample or a more resonant pump frequency would be needed to excite these samples sufficiently to see transient excited state absorption. Higher pump powers could also be used, but only up to a certain point without risking damage to the sample. These simulations also allowed for comparison between theoretical absorption and measured absorption of the experimental samples. While the core/cladding samples showed a discernable difference in absorption for different ion densities, the expected absorption coefficient as predicted by the simulation was 1 to 2 orders of magnitude less, suggesting that a majority of the absorption seen experimentally was due to other factors. These factors could be codopants, which differ between

the cores of each sample. These codopants, such as Al or P, can induce additional vibrational modes which fall in the THz frequency range, and therefore can overshadow the weaker ion absorption. There is also a signal-to-noise ratio issue, which must be improved through higher averaged testing procedures or more optimized samples. These complications lead one to consider what kind of samples would be better suited to these measurements, and what traits they would need to avoid the confounders encountered during this project. The results of the literature search showed that Er- or Nd-doped crystals had both the best intramultiplet spacing and intermultiplet distance for the pump and probe frequencies used in this project, and that $KGd(WO_4)_2$ presents the most attractive host for either ion, as it shows low absorption in both the 800 nm and THz regimes.

Thus, for future efforts concerning this work, a crystalline sample free of codopants presents a much more controlled system to test to see if the absorption from the doped ions is detectable using THz spectroscopy. Also, TRTS presents another avenue for seeing the rare earth response, as the absorption spectrum is predicted to shift as the excited ions relax through the excited multiplet. In order for this effect to be observed experimentally, however, the pumping strength must be improved or a sample with much higher doping concentration must be used; otherwise the absorption features are likely to be so small they are obscured by other features or noise.

In general, this project shows that THz spectroscopy is a useful technique to study the low energy dynamics of these systems. Even given some of the inconclusive results, the THz system has shown that it can identify features and differentiate multiple contributors of absorption, which is the first step in quantifying the response of these complex systems. There is a surprising lack of information on these transitions, which makes this work even more

important, as there may be the possibility for new physics or practical applications hidden in the dynamics of these subsystems.

Bibliography

Information

[1] - Komandin, G. A., Zhukova, E. S., Torgashev, V. I., Boris, A. V., Boris, A. A., Motovilova, E. A., . . . Dressel, M. (2013). Terahertz-infrared spectra of the rare-earth scandate DyScO3 single crystal. J. Appl. Phys. Journal of Applied Physics, 114(2), 024102. doi:10.1063/1.4813496

[2] - Kozlov, G. V., Mukhin, A. A., Pronin, A., Prokhorov, A. S., Zelezny, V., & Petzelt, J. (1990, September 10). Observation of Magnetic Dipole and Electric Dipole Electron Transitions in the Ground Multiplet of the Rare Earth Ion in TmFeO3. Pis'ma Zh. Eksp. Teor. Fiz., 52(5), 890-894.

[3] - Zhang, K., Xu, K., Liu, X., Zhang, Z., Jin, Z., Lin, X., . . . Ma, G. (2016). Resolving the spin reorientation and crystal-field transitions in TmFeO3 with terahertz transient. Sci. Rep. Scientific Reports, 6, 23648. doi:10.1038/srep23648

[4] - Miniscalco, W. (2001). Optical and Electronic Properties of Rare Earth Ions in Glasses. Optical Science and Engineering Rare-Earth-Doped Fiber Lasers and Amplifiers, Revised and Expanded. doi:10.1201/9780203904657.ch2

[5] - Quimby, R. S. (1991). Fluoride glass fiber optics. Academic Press. Chapter 9: "Active Phenomena in Doped Halide Glasses". ed. Aggarwal, I. D., Lu, G.

[6] - Slater, J. C. (1960). Quantum theory of atomic structure (Vol. 1). New York: McGraw-Hill.

[7] - Quimby, R. S. (2006). Photonics and lasers: an introduction. Hoboken, NJ: John Wiley & Sons.

[8] - Wolf, E., Rideburg, L. A., & Weber, M. J. (1976). Progress in Optics XIV. Amsterdam: North-Holland. Chapter III: Relaxation Phenomena in Rare-Earth Luminescence

[9] - Kaminskiǐ, A. A. (1981). Laser crystals: Their physics and properties. Berlin: Springer-Verlag.

[10] - Sethy, P. K., Pratyush, S., Mishra, R., & Behera, S. (2015). An Introduction to Terahertz Technology, Its History, Properties and Application. International conference on computing and communication.

[11] - Hegmann, F., Ostroverkhova, O., & Cooke, D. (2005). Photophysics of Molecular Materials (G. Lanzani, Ed.). 367-417. doi:10.1002/3527607323

[12] - Fornasiero, L., Kück, S., Jensen, T., Huber, G., & Chai, B. (1998). Excited state absorption and stimulated emission of Nd 3 in crystals. Part 2: YVO 4 , GdVO 4 , and Sr 5 (PO 4) 3 F. Applied Physics B: Lasers and Optics, 67(5), 549-553. doi:10.1007/s003400050543

[13] - Pujol, M., Rico, M., Zaldo, C., Solé, R., Nikolov, V., Solans, X., . . . Díaz, F. (1999). Crystalline structure and optical spectroscopy of Er3 -doped KGd(WO4)2 single crystals. Applied Physics B Appl Phys B, 68(2), 187-197. doi:10.1007/s003400050605

[14] - Kuleshov, N. V., Lagatsky, A. A., Podlipensky, A. V., Mikhailov, V. P., Kornienko, A. A., Dunina, E. B., . . . Huber, G. (1998). Fluorescence dynamics, excited-state absorption, and stimulated emission of Er^3 in KY(WO_4)_2. Journal of the Optical Society of America B J. Opt. Soc. Am. B, 15(3), 1205. doi:10.1364/josab.15.001205

[15] - Cornacchia, F., Toncelli, A., Tonelli, M., Favilla, E., Subbotin, K. A., Smirnov, V. A., . . . Zharikov, E. V. (2007). Growth and spectroscopic characterization of Er3 :CaWO4. Journal of Applied Physics, 101(12), 123113. doi:10.1063/1.2749403

[16] - Trevis, J. Appl. Phys. 36, 1033 (1965)

[17] - Walling, Phys. Rev. B 10, 4748 (1974)

[18] - Redfield, D., & Burke, W. J. (1974). Optical absorption edge of LiNbO3. Journal of Applied Physics, 45(10), 4566. doi:10.1063/1.1663089

[19] - Bosomworth, D. R. (1966). THE FAR INFRARED OPTICAL PROPERTIES OF LiNbO3. Applied Physics Letters, 9(9), 330. doi:10.1063/1.1754772

[20] - Shao, Z., Zhang, Q., Liu, T., & Chen, J. (2008). First-principles study on electronic structure and absorption spectra for the CaWO4 crystal with oxygen vacancy. Computational Materials Science, 43(4), 1018-1021. doi:10.1016/j.commatsci.2008.02.013

[21] - Wigmore, J., Kozorezov, A., Rani, H. B., Giltrow, M., Kraus, H., & Taele, B. (2002). Scattering of THz phonons. Physica B: Condensed Matter, 316-317, 589-591. doi:10.1016/s0921-4526(02)00581-1

[22] - Macalik, L., Dereń, P., Hanuza, J., Stręk, W., Demidovich, A., & Kuzmin, A. (1998). Effect of random distribution and molecular interactions on optical properties of Er3 dopant in KY(WO4)2 and Ho3 in KYb(WO4)2. Journal of Molecular Structure, 450(1-3), 179-192. doi:10.1016/s0022-2860(98)00427-x

[23] - Mateos, X., Solé, R., Gavaldà, J., Aguiló, M., Massons, J., & Díaz, F. (2006). Crystal growth, optical and spectroscopic characterisation of monoclinic KY(WO4)2 co-doped with Er3 and Yb3. Optical Materials, 28(4), 423-431. doi:10.1016/j.optmat.2004.12.024

[24] - Han, X., & Wang, G. (2003). Crystal growth and spectral properties of Nd3 :KY(WO4)2 crystal. Journal of Crystal Growth, 247(3-4), 551-554. doi:10.1016/s0022-0248(02)02050-x

[25] - Macalik, L., Tomaszewski, P., Lisiecki, R., & Hanuza, J. (2008). The crystal structure, vibrational and luminescence properties of the nanocrystalline KEu(WO4)2 and KGd(WO4)2:Eu3 obtained by the Pechini method. Journal of Solid State Chemistry, 181(10), 2591-2600. doi:10.1016/j.jssc.2008.06.026

[26] - Kaminskii, A. A., Gruber, J. B., Bagaev, S. N., Ueda, K., Hömmerich, U., Seo, J. T., . . . Kuznetsov, F. A. (2002). Optical spectroscopy and visible stimulated emission of Dy 3 ions in monoclinic $\alpha - KY (WO_4)_2$ and $\alpha - KGd (WO_4)_2$ crystals. Physical Review B, 65(12). doi:10.1103/physrevb.65.125108

[27] - Pujol, M. C., Solé, R., Gavaldà, J., Massons, J., Aguiló, M., Díaz, F., . . . Zaldo, C. (1999). Growth and ultraviolet optical properties of KGd1– xRE x(WO4)2 single crystals. Journal of Materials Research, 14(09), 3739-3745. doi:10.1557/jmr.1999.0505

[28] - Nuss, M., Orenstein, J. Terahertz Time-domain Spectroscopy. Topics in Applied Physics Millimeter and Submillimeter Wave Spectroscopy of Solids, 7-59, doi:10.1007/bfb0103419

Images

(1) - http://www.rareelementresources.com/images/